Direct aqueous carbonation of electric arc furnace slag: process optimisation through experimental design

Materials and Structures (2025) 58:127
https://doi.org/10.1617/s11527-025-02661-6

ORIGINAL ARTICLE

Direct aqueous carbonation of electric arc furnace slag: process optimisation through experimental design

Francesca Bonfante · Giuseppe Ferrara · Pedro Humbert · Davide Garufi · Jean-Marc Tulliani · Paola Palmero

Received: 29 October 2024 / Accepted: 15 April 2025

Abstract At present, one of the strategies to reduce the embodied carbon of cement is to partly replace clinker with metallurgical slags. In this perspective, this study investigates the accelerated aqueous carbonation of electric arc furnace slag as possible treatment for its reuse in the cement industry. In view of developing a low-energy and industrially integrated process, mild carbonation conditions were selected: ambient pressure, low liquid-to-solid ratio, minimised temperature (between 20 °C and 60 °C) and short duration time (ranging from 20 to 60 min). To optimise the carbonation process, a design of experiments was developed. The Response Surface Methodology showed a non-representative trend along time. Therefore, a non-linear model was adopted for a better prediction of CO_2 content above 50 min. The results were satisfactory with an optimum CO_2 uptake of 7.7% and the carbonation degree obtained, 30.2%, was the highest registered in previous literature for open systems. Moreover, a literature analysis on previous aqueous and wet direct carbonation of Electric Arc Furnace slag was carried out using Principal Component analysis. This exploratory data analysis identified the most effective carbonation parameters based on the reactor type and suggested the investigation of further parameters such as liquid-to-solid ratio and CO_2 flow rate and partial pressure, maintaining the perspective of a sustainable process.

Keywords Carbon capture and utilisation · EAF steel slag · Direct aqueous carbonation · CO_2 uptake

F. Bonfante · G. Ferrara (✉) · J.-M. Tulliani · P. Palmero
Department of Applied Science and Technology, INSTM R.U. Lince Laboratory, Politecnico Di Torino, Corso Duca Degli Abruzzi 24, 10129 Turin, TO, Italy
e-mail: giuseppe.ferrara@polito.it

F. Bonfante
e-mail: Francesca.bonfante@polito.it

J.-M. Tulliani
e-mail: jeanmarc.tulliani@polito.it

P. Palmero
e-mail: paola.palmero@polito.it

P. Humbert · D. Garufi
CRH Innovation EMAT, De Klencke 10-12, 1083 HL Amsterdam, The Netherlands
e-mail: phumbert@crh.com

D. Garufi
e-mail: dgarufi@crh.com

Published online: 26 April 2025

1 Introduction

Within the industrial sector, the steelmaking and cement industries are acknowledged as the primary contributors to global CO_2 emissions, accounting for about 15% of total anthropogenic carbon release [1]. In order to mitigate its impact, the cement industry has identified a range of industrial by-products that can be employed as partial substitutes for clinker, which is responsible for the majority of emissions associated with its production. Among

these by-products, granulated blast furnace slag is extensively utilised [2] and can substitute up to 95% of clinker [3]. At the same time, steelmaking industry is implementing adaptive strategies to reduce its emission, shifting towards more sustainable processes. Figure 1, adapted from [4–6], illustrates the generation process of various types of slags derived from cast iron and steel production. Blast furnace slag is generated as a by-product of the ironmaking process, which is a necessary precursor to the steelmaking process through the Basic Oxygen Furnace (BOF). The latter produces BOF slag that is considered to have lower hydraulic properties with respect to blast furnace slag [7]. The electric process, which commences with steel scrap and avoids the utilisation of molten iron, is being adopted on an ever-growing larger scale. Over the course of a decade, global production of electric arc furnace (EAF) steel increased from around 452 million tonnes in 2012 to 531 million tonnes in 2022 [8, 9]. This process generates huge amounts of slag, and precisely ≅ 120 to 170 kg per ton of steel produced [10].

EAF slag can be classified according to the different typologies of steel, with the designation EAF-C applied to slag derived from carbon steel production and EAF-S to that produced from stainless/high alloy steel. The composition of EAF slag is highly variable due to the addition of different compounds and due to the heterogeneity of the feed material, particularly of the steel scrap. Literature has been focusing on different routes for treatment and reuse of EAF slag, including its application in asphalt mixtures [10], as a filler in nitrile butadiene rubber [11], as inert material [12] and aggregates [13], with particular emphasis on its use in the construction sector [5]. However, the large-scale reuse of EAF slag is still under investigation due to some challenges, namely its alkaline composition, the high-volume instability and the possible leaching of hazardous metals [5, 14, 15].

A smart approach implies the accelerated carbonation of steelmaking slag, which combines the CO_2 storage to volume stabilisation [16], demonstrating both economic and environmental benefits [2]. For these reasons, many studies have focused on direct EAF slag mineralisation aiming at maximising the degree of carbonation of EAF slag and its stabilization for further reuse. Research on direct carbonation of EAF slag started by studying the CO_2 sequestration capacity of a slag suspension along with time and at ambient conditions [17]. Subsequently, Baciocchi et al. [18] compared the performances of EAF slag carbon capture in different configurations, i.e. wet (liquid-to-solid ratio < 1.5) and aqueous carbonation (liquid-to-solid ratio > 5), at high temperatures and pressures. Omale

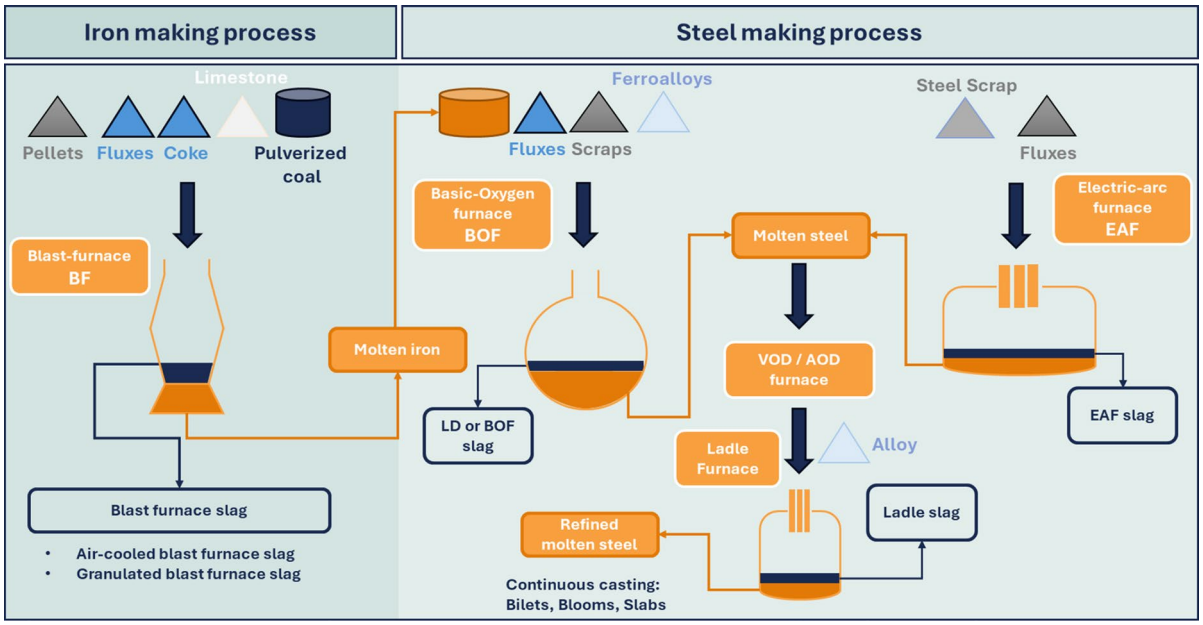

Fig. 1 Iron and steel making processes and steel slags generation

et al. [19] studied the effects of reaction time, pressure and liquid-to-solid ratio on a Malaysian EAF slag. However, these studies considered only one parameter at a time, thereby neglecting the potential interactions between them. Only a limited number of studies have employed a multivariable approach [20]. Pan et al. [21] investigated the combined effect of temperature, rotating speed and slurry flow rate in a rotating packed bed reactor, while Ibrahim et al. [22] examined the effect of gas flow rate, liquid-to-solid ratio and inert particles fraction in an inert-particles spouted bed reactor. Although the positive correlation of time and the accelerating effect of temperature on the reaction kinetics have been previously observed, the mutual interaction between time and temperature has never been investigated. This aspect is crucial for the purposes of a costs-benefits analysis and process optimisation.

To cover this gap in knowledge, this paper aims to study the effects of direct aqueous carbonation on EAF slag properties and composition, with a particular focus on the combined effect of time and temperature. These parameters were selected as significantly affecting the sustainability of the carbonation process. In the context of developing an industrially integrated low-energy process, only mild carbonation conditions were investigated. Multivariate principal component analysis was proposed as a means of taking a comprehensive look at the literature on wet carbonation of EAF slag. This innovative approach allowed for a summary and discussion of the significance and effect of carbonation parameters and setups.

2 Materials and methods

2.1 Materials characterisation

Electric Arc Furnace slag was collected from steelmaking manufacturing at the downstream EAF unit from carbon steel production, meaning an EAF-C slag typology. The initial granulometry of the material was in the range 0–6 mm. Grinding and milling processes reduced the grain size to a maximum diameter of 50 µm, providing the slag designated as *as-received*. The material's chemical composition was assessed using Rigaku Supermini 2000 X-ray fluorescence spectrometer (Rigaku, Japan) and reported in Table 1. The main elements observed in the slag, conventionally expressed as oxides, were Fe_2O_3, CaO, SiO_2 and Al_2O_3. Significant amounts of magnesium and manganese oxides were detected as well.

Based on the material's chemical composition, the carbonation potential ($ThCO_2$) can be calculated according to Eq. (1) [23].

$$\%ThCO_2 = 0.785\left(\%CaO - 0.56 \cdot \%CaCO_3 - 0.7 \cdot \%SO_3\right) + 1.091 \cdot \%MgO + 0.71 \cdot \%Na_2O \quad (1)$$

EAF slag carbonation potential resulted in 25.4%, considering the calcium carbonate percentage, as discussed in paragraph 3.1**.**

X-ray diffraction analysis was used to identify crystalline phases. The X-ray diffractometer Malvern Pan'alytical Empyrean (Malvern Pan'alytical, The Netherlands), in Bragg–Brentano configuration, was equipped with a copper anticathode ($CuK\alpha_1$ radiation, $\lambda = 0.154056$ nm) operating at 40 kV and 40 mA, and a PIXcel detector. 2θ spanned from 5 to 70° with an angular step of 0.006° held for 23 s.

The particle size distribution before and after the carbonation was characterised through laser granulometry (Malvern Mastersizer 3000 AERO S, UK).

Thermogravimetric/Differential Thermal Analysis (TG–DTA, LABSYS EVO from Setaram, France) was used for qualitative and quantitative evaluation of changes in the material composition. Analyses were carried out up 1050 °C at a rate of 10 °C/min in alumina crucibles with N_2 as carrier gas at a flow rate of 20 L/min.

Particles' morphology was characterized using Phenom XL scanning electron microscope (SEM, Phenom, Ambler, PA, USA) equipped with an energy-dispersive X-ray spectroscopy (EDS) detector and operating at 15 kV accelerating voltage. Before SEM characterisation, as received and carbonated EAF slag samples were coated with a layer of gold (about 30 nm) using SPI Module sputter.

Table 1 Chemical composition of as-received slag by XRF analysis

Chemical composition (wt.%)											
Na_2O	MgO	Al_2O_3	SiO_2	P_2O_5	SO_3	CaO	TiO_2	MnO	Fe_2O_3	Other	LOI
0.11	5.35	10.50	16.20	0.54	0.30	27.10	0.55	4.74	30.80	0.71	3.11

2.2 Direct aqueous mineralisation and CO_2 uptake

The equipment employed for the mineralisation process was previously described in Bonfante et al. [24] and is illustrated in Fig. 2. The carbonation set-up consisted of a glass flask (500 mL), a crystalliser, a magnetic stirrer with a hot plate and the CO_2 bottle, which was connected to the flask by a tube. To ensure temperature control, the flask was immersed in a crystalliser. Aqueous carbonation was performed by mixing 80 g of fine EAF slag powder and 240 mL of deionized water. The fixed parameters adopted for aqueous carbonation were ambient pressure, a liquid-to-solid ratio (L/S) of 3, and a 99.9% CO_2 flow rate (FR) of 150 L/h. Reaction time and temperature were varied to study their effect on the EAF slag carbonation efficiency. Indeed, the flask was sealed with a cap that had been drilled to facilitate the passage of the CO_2 tube in order to mitigate water evaporation at elevated temperatures. This ensured that, despite the system's open configuration, water evaporation and, consequently, variations in the L/S ratio were negligible. The slurry obtained following carbonation was subjected to centrifugation, and the separated residue was subsequently dried in an oven for a period of 24 h at a temperature of 60 °C (see Fig. 2). This temperature was selected to prevent the partial loss of C-S–H bound water. The dried specimens were constituted of a fragile slag residue that was readily pulverised without necessitating further mechanical reduction.

Two methods were employed to quantify the CO_2 content, following the authors' previous studies [25, 26]: Thermogravimetric-Differential Thermal Analysis (TG–DTA) and thermal decomposition in a furnace. TG–DTA and thermal decomposition allow the quantification of CO_2 as weight loss occurring between 550 °C and 850 °C, where complete calcium carbonate decomposition occurs [27–29]. The CO_2 content (m_{CO_2}) is quantified through Eq. (2), in which $m_{550\,°C}$ and $m_{850\,°C}$ are the mass of the sample, respectively measured at 550 °C and 850 °C, while m_i is the mass of the sample before the thermal treatment. For both methods the measurements were repeated three times.

$$m_{CO_2}(\%) = \frac{(m_{550°C} - m_{850°C})}{m_i} \cdot 100 \quad (2)$$

Based on these CO_2 quantification techniques, the literature agrees with the adoption of Eq. (3) for calculating CO_2 uptake. This equation describes the CO_2 captured material's initial mass, assuming that the CO_2 captured is the only contribution to the mass gain.

$$\%CO_{2\,\text{uptake}} = \frac{\Delta CO_2}{m_i} \cong \frac{m_{CO_2\text{carbonated}} - m_{CO_2\text{initial}}}{1 - m_{CO_2\text{initial}}} \quad (3)$$

In order to compare the results from different studies, the carbonation degree, denoted as η_{ca} and

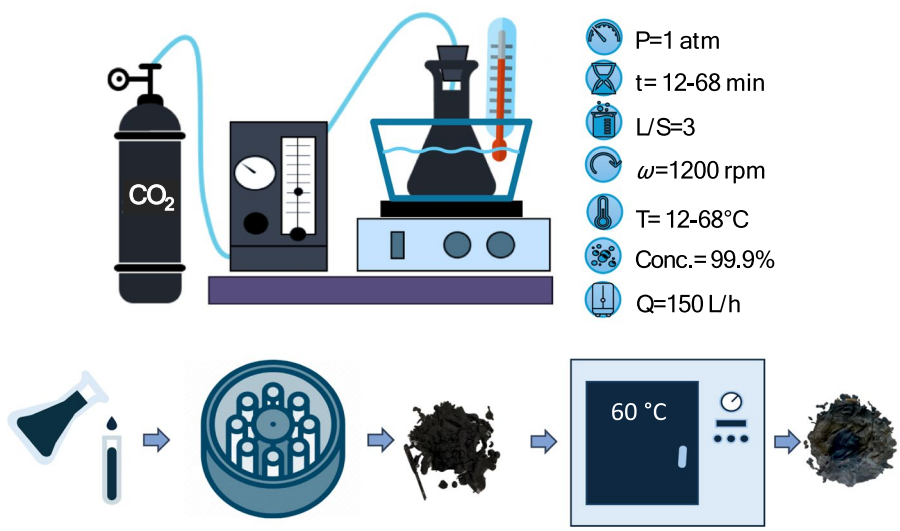

Fig. 2 Experimental set-up adopted for aqueous carbonation

expressed as the ratio between the CO_2 uptake and the carbonation potential (Eq. (4)), is preferably used.

$$\eta_{ca}(\%) = \frac{\%CO_{2\,uptake}}{ThCO_2} \cdot 100 \quad (4)$$

were $ThCO_2$ is the theoretical CO_2 uptake assessed by Eq. (1).

2.3 Design of experiment

In order to optimize the mineral carbonation parameters, a Design of Experiments (DoE) was developed through Minitab software (Minitab, PA, USA). A set of ten experimental runs was designed using Response Surface Methodology (RSM). The RSM approach is based on maximizing the information with a minimum number of experiments conducted [30]. A Central Composite Design (CCD) was selected to analyse how the two independent variables, reaction time (min) and temperature (°C), affect the system response (i.e. the CO_2 content after carbonation). The experimental design space created consisted of a temperature varying between 20 °C and 60 °C and a reaction time between 20 and 60 min, a timeframe that can be integrated into industrial processes. The experimental points investigated, and the corresponding coded units are reported in Table 2. The CO_2 content of the mineralized EAF slag, after the eleven experiments generated by RSM, was quantified by thermal decomposition.

2.4 Multivariate principal component analysis

Principal Component Analysis [31] is a tool for unsupervised exploratory data analysis. The objective of the analysis was to facilitate a comparative assessment of the findings from various literature studies, which considered different operational parameters. The application of this decomposition technique allows for the reduction of the number of variables of the starting domain by deriving a new set of variables, the so-called Principal Components (PCs), obtained from a linear combination of the initial variables. The first PC is selected along the direction of maximum variance in the data, and the following orthogonal components are selected to maximize the variance at every step. Equation (5) represents the PCA decomposition equation.

$$\mathbf{X} = \sum_{f=1}^{F} \boldsymbol{t}_f \cdot \boldsymbol{p}_f^T + \mathbf{E} = \mathbf{T}\mathbf{P}^{\mathrm{T}} + \mathbf{E} = \hat{\boldsymbol{X}} + \mathbf{E} \quad (5)$$

in which X is the matrix of the original data, while $\hat{X}$ represents the modelled matrix, F is the number of PCs, t and p represent respectively scores and loadings (the two vectors that describe each PC), while E describes the unmodeled part, also called the "residuals".

Principal Component Analysis was performed using the PCA toolbox (for MATLAB) [32] under MATLAB software (2017b, Mathworks, MA, USA) environment.

3 Result and discussion

3.1 Effects of carbonation on EAF slag properties and composition

The granulometric curves of EAF slag, before and after the carbonation process, are depicted in Fig. 3. Both materials exhibited a monomodal distribution. However, as-received EAF slag showed pronounced inflection points, and was characterized by D10, D50 and D90 values of 1.5 µm, 9.4 µm and 24.1 µm, respectively. Following the carbonation process, the distribution of particles was observed to undergo a reduction in the frequency of the finest particles, which is likely attributed to agglomeration. The D10, D50 and D90 values were recorded as 3.6 µm,

Table 2 Coded levels of each parameter with corresponding real values used in CCD

Parameter	Extreme minimum ($-\sqrt{2}$)	Low (−1)	Center (0)	High (+1)	Extreme maximum ($+\sqrt{2}$)
Temperature (°C)	12	20	40	60	68
Time (min)	12	20	40	60	68

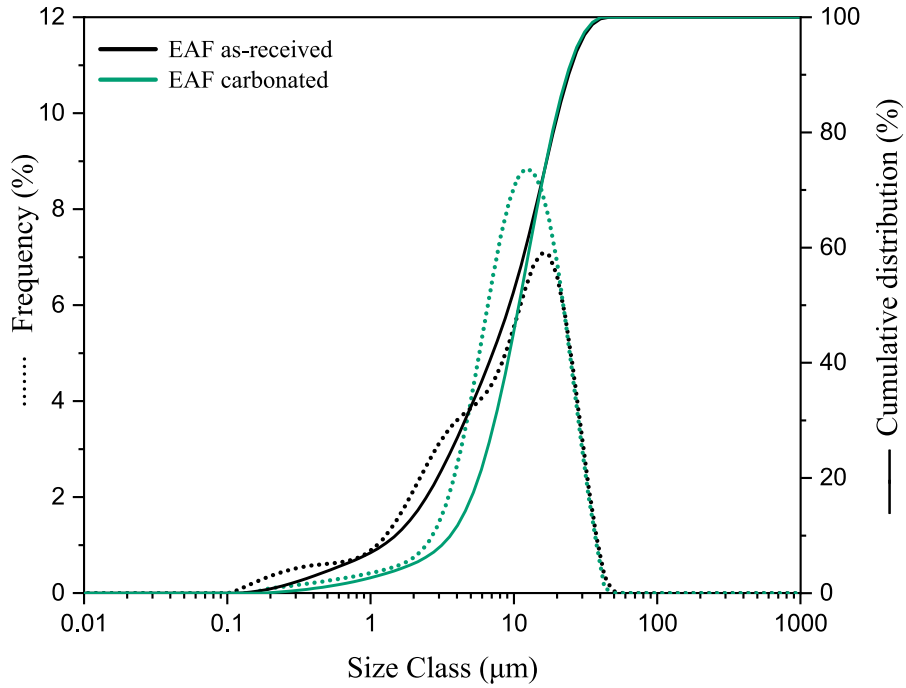

Fig. 3 Particle size distribution of as received and carbonated EAF slag

10.8 μm and 23.5 μm, respectively. Overall, the particle size of the EAF slag, both before and after carbonation, was found to be comparable to the typical particle size distribution of cement, although slightly finer.

XRD patterns of as-received and carbonated EAF slag are displayed in Fig. 4. As-received EAF slag was mainly composed of iron oxide (FeO), aluminosilicates (i.e., akermanite, $Ca_4MgAl_3SiO_{14}$, and gehlenite, $Ca_2Al_2SiO_7$), larnite (Ca_2SiO_4) and merwinite ($Ca_3MgSi_2O_8$). Besides, low intensity signals attributable to calcite ($CaCO_3$) and iron manganese oxide (Fe_2MnO_4) were also detected. After the carbonation, the peaks related to calcium carbonate showed an increased intensity. On the other hand, larnite was no more detected, confirming the participation of this compound in the reaction described by Eq. (6), as previously observed in other studies [6, 33]. Peaks related to merwinite were also less intense in the carbonated sample indicating a possible involvement in the reaction. In fact, merwinite can react with CO_2 to form calcium/magnesium carbonates (Eq. 7). However, no magnesium carbonate is detected in the carbonating powder. As shown in studies analysing the carbonation of steel slag in autoclave conditions, merwinite is the slowest mineral to carbonate and can result in the production of non-carbonate amorphous matter [34]. Given the mild operating conditions adopted in this study and the absence of merwinite peaks after the carbonation, partial carbonation of merwinite to form calcium carbonate and an amorphous phase would be consistent with the literature.

$$\left(2CaO \cdot SiO_2\right) + 2CO_2 \rightarrow 2CaCO_3 + SiO_2 \quad (6)$$

$$Ca_3MgSi_2O_8 + 4CO_2 \rightarrow 3CaCO_3 + MgCO_3 + 2SiO_2 \quad (7)$$

As expected, the other phases did not show any reactivity towards carbonation under the mild conditions tested.

TG–DTA curves of EAF slag are reported in Fig. 5. These measurements were essential for confirming the validity of the selected temperature range, particularly in preparation for the thermal decomposition measurements. Furthermore, TG–DTA analysis ensured the absence of other carbonates, such as magnesium carbonate, that might influence the correct temperature range to inspect. The initial content of CO_2 ($m_{CO2\ initial}$), obtained from the TG curve in the 550 °C–850 °C range, resulted in 1.6% (±0.2%), providing an average

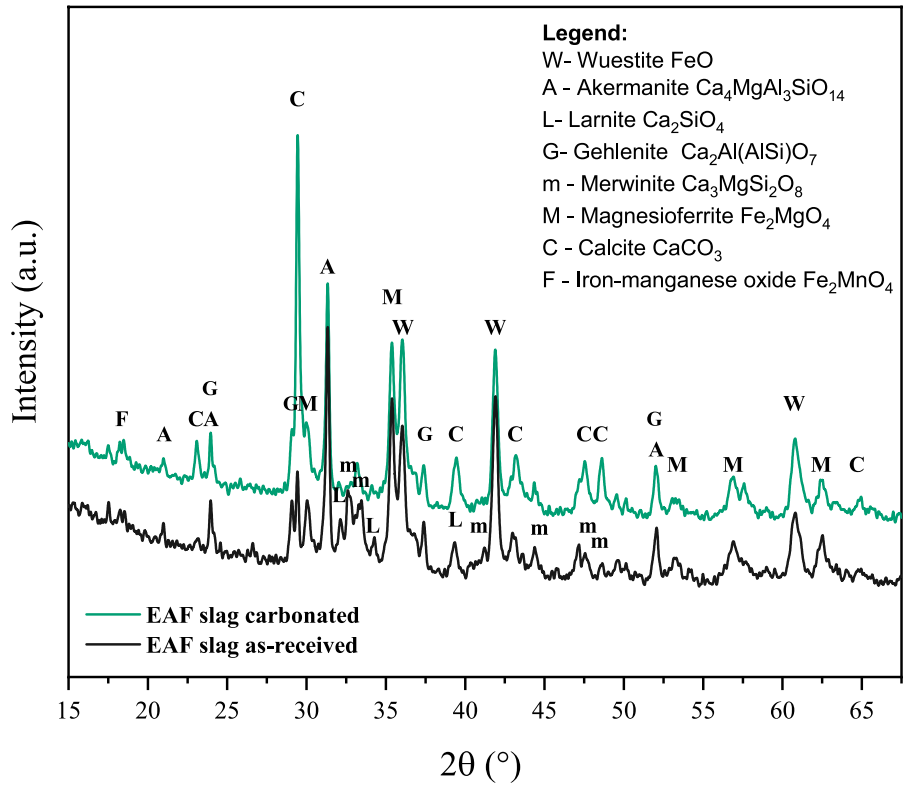

Fig. 4 XRD pattern (Cu-Kα1 radiation λ = 0.154056 nm) of as received (black) and carbonated (green) EAF slag. *Reference codes: W – 96–900-8637, A – 96–900-6115, L – 96–901-2791, G – 96–101-1003, m – 96–900-0286, M – 96–900-3624, C – 00–005-0586, F – 96–230-0619*

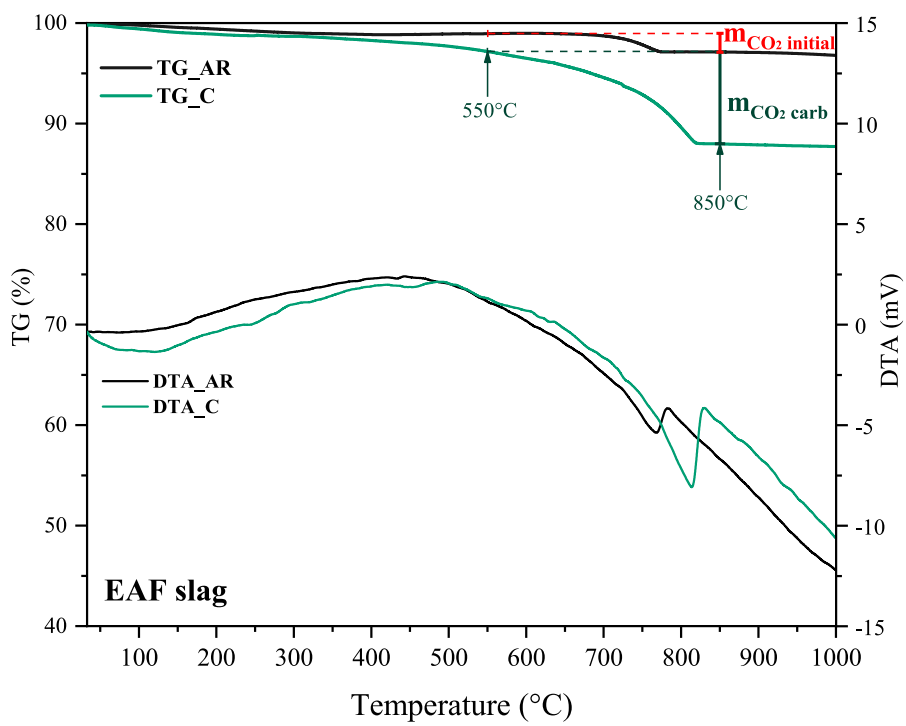

Fig. 5 TG and DTA curves of as-received (black) and carbonated (green) EAF slag

$CaCO_3$ content of 3.7 wt%. The content of CO_2 visibly increased after 1 h of carbonation ($m_{CO2\ carb}$) at ambient temperature (~ 20 °C), reaching an average value of 8.8% (± 0.6%). Due to the increased content of carbonates, it is also possible to observe a shift in the DTA peak of calcium carbonate from 765 °C of as-received slag to 815 °C of carbonated slag [35].

Figure 6 shows the SEM observations of EAF slag before and after the carbonation process. Before the carbonation, the surface of the particles appears generally smooth (Fig. 6 a and b) and characterized by sharp edges. After the carbonation, it's possible to observe fine precipitates on the particles' surface (Fig. 6 c and d). In order to better characterise the surface chemistry of these particles, EDX analysis was carried out on the different morphologies individuated. Figure 7 provides the energy dispersive X-ray spectroscopy (EDS) spectra for each point analysed and the corresponding elemental weight percentage. Point 1 is positioned on the smooth surface of an EAF slag particle: the elemental analysis provided O, Ca, Si and Al as the main elements (Fig. 7a), attributable to calcium silicates and aluminosilicates. EDX analysis on Point 2 showed the presence of Fe in a significant amount (Fig. 7b), suggesting the positioning on an iron oxide agglomerate. Point 3 is located on the small precipitates on the surface of the carbonated material: here the neat predominance of O and Ca elements (Fig. 7c) makes it possible to associate such precipitates to the calcium carbonate phase, in agreement with previous studies [36]. Point 4 is positioned on the same particle, but in a region where less precipitates are present: here Ca, O and Si have the highest atomic percentage, suggesting the occurrence of carbonation on a calcium silicate particle, in agreement with XRD results (Fig. 7d).

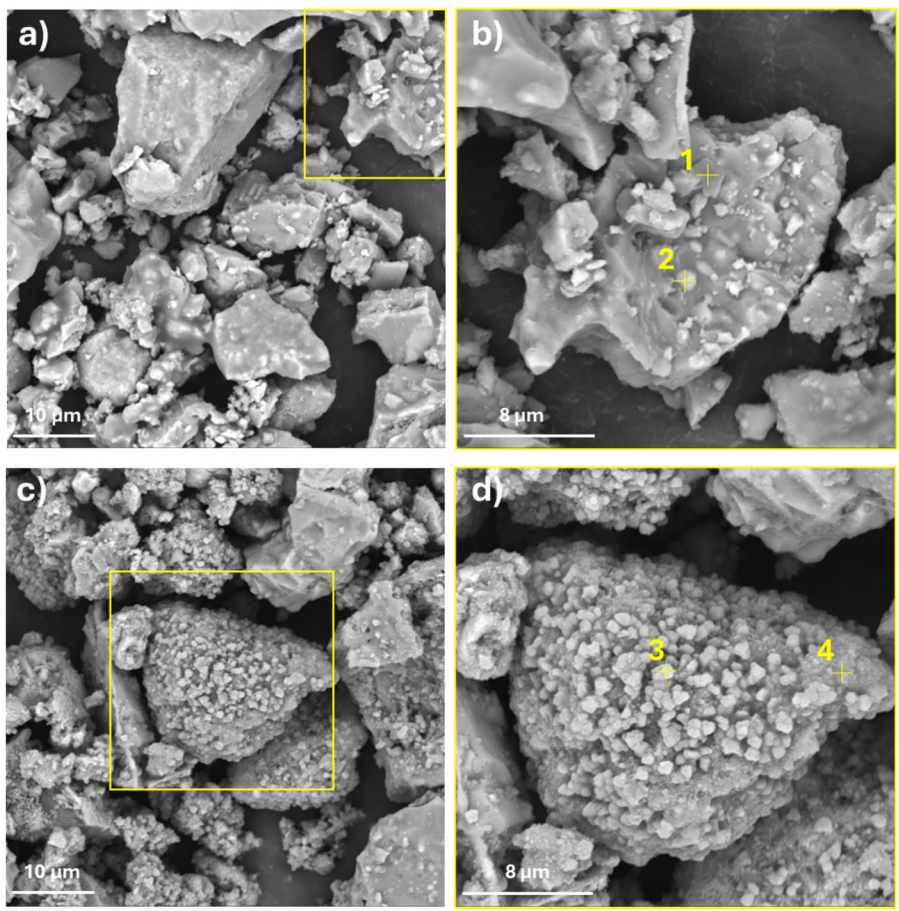

Fig. 6 Scanning electron microscopy of EAF slag as received **a**, **b** and carbonated **c**, **d** at lower (a, c) and higher (b, d) magnifications

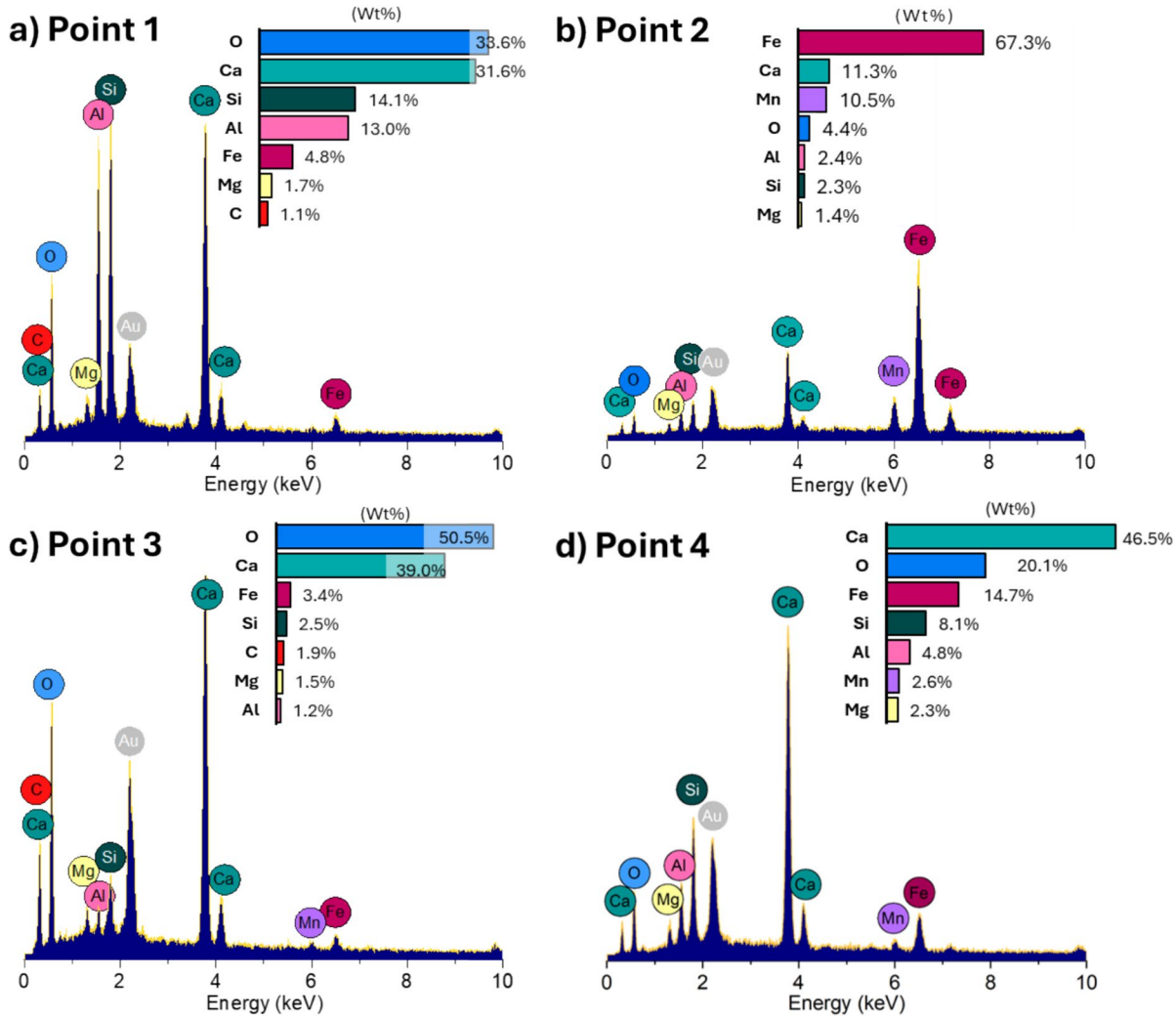

Fig. 7 EDX analysis of the points identified in EAF slag as-received **a** and **b** and carbonated **c** and **d**

3.2 Response surface methodology and non-linear models

The adoption of RSM and CCD allows the simultaneous study of the two parameters and their interactions. The 10 measurements of CO_2 content, selected according to the CCD and calculated with the thermal decomposition using Eq. (2), are listed in Table 3. The experiment of the central point (EAF3) was repeated two times.

The linear model regression (Eq. (8)) accounts for 86.3% of the variance (R^2), with a standard error (S) of 0.45%.

$$CO_2\ \text{content}(\%) = 3.78 + 0.1162 * T + 0.1183 * t - 0.0017 * T^2 - 0.0011t^2 \quad (8)$$

Although both the variance and the standard error are within acceptable limits and the model can fit the experimental data points with reasonable accuracy, this equation has a limit after a certain reaction time. In fact, it is possible to identify a maximum CO_2 content within the experimental space, specifically at 33 °C and 52 min, which results in a decline in CO_2 uptake after 52 min, while it is expected to follow an asymptotic trend [19, 22]. In order to have a suitable trajectory at higher reaction time, a non-linear

Table 3 Experimental values of CO_2 content (%) obtained from EAF slag along with their percent errors

Obs	Uncoded units		Coded units		CO_2 content (%)	
	T(°C)	t(min)	X-T(°C)	Y–t(min)		
EAF1	20	60	−1	1	8.36%	±0.06%
EAF2	20	20	−1	−1	7.51%	±0.08%
EAF3	40	40	0	0	8.47%	±0.05%
EAF3B	40	40	0	0	8.61%	±0.02%
EAF4	60	20	1	−1	6.06%	±0.37%
EAF5	60	60	1	1	6.87%	±0.05%
EAF6	11.72	40	$-\sqrt{2}$	0	7.61%	±0.06%
EAF7	40	11.72	0	$-\sqrt{2}$	6.89%	±0.05%
EAF8	68.28	40	$\sqrt{2}$	0	7.07%	±0.02%
EAF9	40	68.28	0	$\sqrt{2}$	8.75%	±0.11%
EAFopt	**35**	**60**	**−0.25**	**1**	**8.63%**	**±0.07%**

regression (NL-reg) model based on the same dataset was proposed (Eq. (9)).

$$CO_2\ \text{content}(\%) = \frac{7.6336 \cdot t}{5.40943 + t} + 0.103403 \cdot T - 1.58273E - 3 \cdot T^2 \quad (9)$$

Standard error (0.45) and optimum temperature (33 °C) of this new model were found to be equivalent to those of the linear model, thought, in this case, the CO_2 content trend is better described as the new equation predicts its continuous increase along with the reaction time. Figure 8 illustrates the predicted CO_2 content values, as calculated using the NL-reg model (Eq. (9)). The predicted optimum temperature and the highest reaction time within the experimental space are highlighted in red. Equation (9) suggests

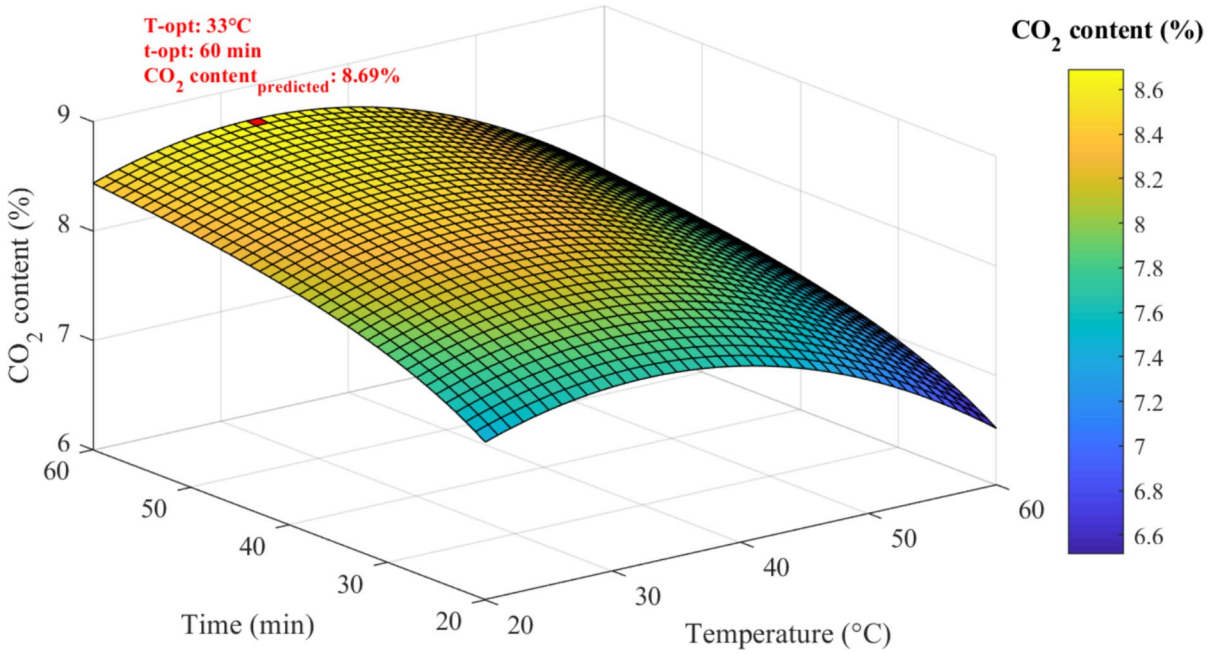

Fig. 8 3D response surface plot of CO_2 content of EAF slag: effect of time and temperature at ambient pressure, L/S = 3, FR = 150 l/h

that the CO_2 content increases by approximately 7% during the initial hour of carbonation, and then by a mere 0.3% during the subsequent hour. Consequently, the maximum reasonable reaction time was set at 60 min, and the investigation space was not extended.

Based on the optimum conditions identified, a further experiment was conducted at 35 °C and 60 min (EAFopt, in Table 3) to verify the prediction of the models. The CO_2 content at optimum conditions resulted of 8.63%, while the predictions of the linear and non-linear models were 8.78% and 8.69%, respectively. The non-linear model better fits the experimental data, which, however, stays within the confidential interval (95%) in both the models' predictions. The two models exhibit a comparable trajectory below 30 min.

To separately investigate the effect of time and temperature on the carbonation degree, representative curves are shown in Fig. 9 fixing one of the two considered operational parameters. Specifically, curves fitting both linear (Fit-L) and non-linear (Fit-NL) regression models are reported as well as the experimental point data. Considering the effect of time on the carbonation rate (Fig. 8 a–c), it is possible to observe the typical asymptotic trajectory of the CO_2 content. This behaviour is consistent regardless of temperature, which seems to affect the carbonation efficiency but not the asymptotic trend. In fact, as confirmed by previous studies [19, 22], the carbonation degree is directly proportional to the reaction time until a plateau is reached, which is caused by the saturation of the carbonated material.

Figure 8d–f show that both models can correctly predict the parabolic trajectory of CO_2 content along with the temperature axis and that this trend is not affected by the reaction time. The effect of temperature has been mainly studied in pressurised environments, where it is known to be directly proportional to the CO_2 uptake [18, 36, 37]. In this study, the carbonation process was conducted in an open system. Therefore, two opposing effects can be expected with increasing temperatures. It has been demonstrated that elevated temperatures facilitate the rate of the calcium dissolution reaction [21], thereby enhancing its availability for carbonation. Conversely, the solubility of CO_2 in the slurry decreases with temperature increase. Thus, an arc trend is going to describe the effect of temperature on the CO_2 uptake, depending on the specific kinetic of the material under study.

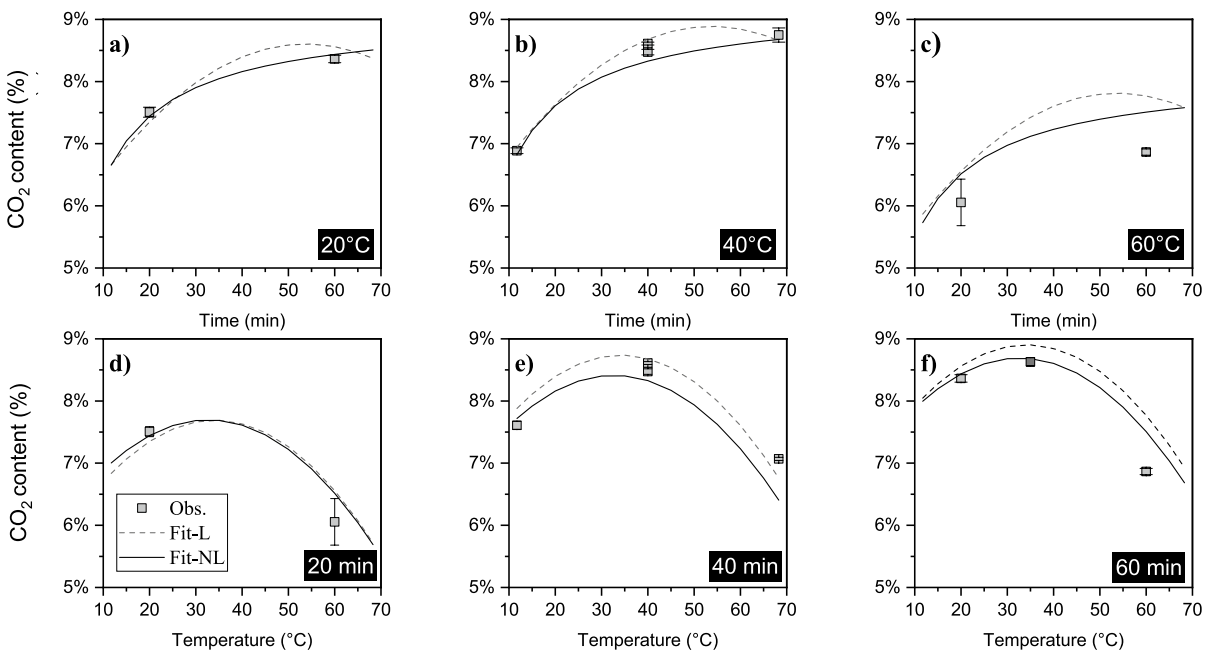

Fig. 9 Interaction plot of the experimental observations (Obs.), the linear regression model (Fit-L) and the non-linear regression model (Fit-NL)

The optimum temperature value is defined by a threshold above which the carbonation rate diminishes. This is a crucial aspect to consider in view of industrial applications aimed at optimising the efficiency of the process.

It is worth to emphasise that the model can be adopted to optimise the proposed mineralisation process by considering the mutual interaction between the operational parameters, i.e. time and temperature. For instance, elevating the temperature from 20 °C (Fig. 8 a) to 40 °C (Fig. 8 b) enables a reduction in reaction time by 50% while obtaining a CO_2 content almost unchanged (with values of 8.4% and 8.1%, respectively). This data can provide valuable support in defining future applications to optimise the process not only in terms of CO_2 content but also in terms of the process carbon footprint. In fact, the potential applications of this study are designed to utilise industrial flue gases, rich in CO_2 content, that have already reached such temperatures. In addition, the exothermic process of carbonation itself also generates suitable temperatures for large volumes of slurry that should be not neglected.

A detailed Life Cycle Assessment analysis could incorporate this information together with the other processes involved and quantify the beneficial contribution in terms of CO_2 emission reduction. In particular, the overall CO_2 cut needs to balance the involved energy-demanding steps. In this regard, the transport of EAF slag from the production site to the carbonation plant could prove to be a high carbon footprint step. Similarly, the grinding pre-treatment, the drying of the material and the treatment of the residual solution can be considered as energy-intensive processes.

A possible effective application is represented by a well-designed integration of the wet carbonation process into the cement production plant. This not only would contribute to optimise the treatment of the residual material, by providing filter press, and allowing the redirection of high temperature gases in the slag drying step, but it also would promote the use of the carbonated product as supplementary cementitious material. A previous study by the authors [38] highlighted that the most significant impact in terms of reducing the carbon footprint will be derived not only from the CO_2 uptake of the EAF slag, but also from its final reuse, particularly in the case of partial cement substitution.

3.3 CO_2 uptake and literature comparison

The CO_2 uptake at the optimum point (identified at 35 °C and 60 min) was calculated from Eq. (3), and resulted in 7.7%. Nevertheless, the comparison with literature does not solely rely on CO_2 uptake; the carbonation degree is also a useful parameter in this regard. Indeed, it facilitates the comparison of the extent of the carbonation process based on the amount of reactive compounds available in the original material. The carbonation degree was calculated from CO_2 uptake and $ThCO_2$ using Eq. (5). With a carbonation potential of 25.4%, obtained through Eq. (1) from XRF and TG analyses, the corresponding carbonation degree was approximately 30%. Table 4 presents a list of previous aqueous and wet carbonation studies on EAF slags carried out in different reactors and carbonation conditions. For the purposes of this study, only a selection of experiments was included, specifically the cube, central and optimum points (i.e. EAF1-5 and EAFopt). Before analysing the data in more detail, it is worth noting that the degree of carbonation (η) achieved in this study was the highest recorded in the literature for open systems.

As shown in this table, there is a large number of parameters affecting the CO_2 uptake and the carbonation degree. Furthermore, the variety of configurations and conditions employed complicates the process of analysis and comparison of the results. Consequently, this study proposes an exploratory analysis through PCA, which facilitates the analysis of a multivariate dataset by reducing the original variables into a smaller number of new variables. This method facilitates the visualisation of system variability, allowing for the identification of both which parameters are significantly affecting the response and the nature of this effect. The model was built on the 32 experiments listed in Table 4, including 7 variables. The variables can be divided into input and output parameters. Input parameters are the set conditions: temperature (T), CO_2 partial pressure (Conc.), time (t), liquid-to-solid ratio (L/S) and flow rate (FR); while the output parameter selected is the carbonation degree (η). The particle size, which is a fundamental parameter for the carbonation, was not included due to the lack of representative data. In fact, the values reported in the literature studies refer to the maximum particle size of the tested materials, therefore not representative of the actual granulometric distribution.

Table 4 Literature comparison in terms of reactor type, PS: maximum particle size, T: temperature, Conc.: CO_2 partial pressure, P: pressure, t: time, L/S: liquid to solid ratio, FR: flow rate, CO_2 uptake, $ThCO_2$: carbonation potential, η: carbonation degree and other parameters

	Ref	Reactor	PS [1] (μm)	T (°C)	Conc. (%)	P (bar)	t (h)	L/S	FR (L/h)	CO_2 uptake (%)	Th CO_2 (wt.%)	η [2] (%)	Other
1	[17]	Open system	106	20	15	1	24	10	0.3	1.70	36.7	4.6	24 h agitation before carbonation
2	[43]	PSSR [3]	150	50	100	1	2	0.4	0	15.50	42.3	36.6	
3	[18]	PSSR	150	50	100	10	1	10	0	7.00		16.5	
4			150	50	100	10	4	10	0	11.00		26.0	
5			150	150	100	10	2	10	0	13.00		30.7	
6			150	50	100	19	2	10	0	10.00		23.6	
7			150	100	100	10	4	10	0	14.00		33.1	
8			150	50	100	1	1	0.4	0	9.00		21.3	
9			150	50	100	3	4	0.4	0	17.00		40.2	
10			150	50	100	10	1	0.4	0	12.50		29.5	
11	[40]	Open system	100	25	15	1	1.1	10	50	8.70	49	17.7	EAF slag type A
12		Open system	100	25	15	1	1.1	10	50	1.90	41.8	4.5	EAF slag type B
13	[37]	PSSR	150	100	100	10	24	5	0	28.00	42.3	66.1	
14			150	100	100	10	1	5	0	18.50		43.7	
15			150	50	100	10	24	0.3	0	17.60		41.6	
16	[44]	PSSR	24	20	18	8	0.33	2.5	0	1.30	36.3	3.6	Gas/Liquid = 2
17	[21]		15	25	100	1	0.67	25	150	17.50	47.1	37.2	Slurry flow rate = 1 L/min
18		RPBR[4]	15	60	30	1	0.67	25	150	25.00		53.1	Slurry flow rate = 0.75 L/min
19			15	55	100	1	0.67	25	150	38.00		80.7	Slurry flow rate = 0.6 L/min
20	[22]	IPSBR[5]	250	25	10	1	15.3	17.5	42	10.60	33.1	32.0	Deionized water
21			250	25	10	1	15.3	17.5	42	22.00		63.5	Solution conductivity = 100–120 ms/cm
22	[19]	PSSR	63	20	100	1	1	5	0	2.79	17.9	15.6	
23			63	20	100	5	3	5	0	5.84		32.5	
24	[36]	SCC[6]	105	70	100	90	48	0.4	0	17.20	28.4	60.6	30 min hydration; Supercritical CO_2
25			105	70	100	101	48	0.4	0	21.34		75.2	
26	[45]	PSSR	76	20	20	2	2	5	0	2.29	35	6.6	Sodium citrate 0.20 mM/L
27	This study	Open system	51	20	100	1	1	3	150	7.36	25.4	29.0	
28			51	20	100	1	0.33	3	150	6.36		25.0	
29			51	40	100	1	0.67	3	150	7.65		30.1	
30			51	60	1.00	1	0.33	3	150	4.72		18.6	
31			51	60	1.00	1	1	3	150	5.63		22.2	
32			51	35	1.00	1	1	3	150	7.67		30.2	

[1]PS, declared maximum particle size; [2]Carbonation degree, calculated based on the $ThCO_2$ obtained from the XRF available and based on Eq. (1); [3]PSSR, Pressurised Stainless Steel Reactor; [4]RPBR, Rotating Packed Bed Reactor; [5]IPSBR, Inert Particles Spouted Bed Reactor; [6]SCC, Supercritical CO_2 Autoclave Reactor.

For what concerns the output parameter, the carbonation degree was preferred with respect to the CO_2 uptake thanks to the incorporation of the $ThCO_2$, which allowed to partially eliminate from this system the great variety of composition typical of EAF slags. However, the CO_2 uptake was integrated as response of the model. After the matrix selection, the data are standardised and it is possible to evaluate the best number of PC, based on their eigenvalue (> 1), the cumulative variance (> 80%), as in accordance to literature [39], and the corresponding minimum root mean square error of cross-validation. These three conditions were satisfied for 4 PCs (see Fig. 10). The explained variance (EV) of the so-obtained PCA model accounted for 89.7%. The information modelled by PCA were first inspected by looking at the loadings plot, which shows the relations among the original variables and the new PCs. PCs, in fact, can be interpreted as new axes from which it is possible to evaluate the data with the best angle.

Only PC1 and PC2 are shown in Fig. 11 since the aim of this analysis was to identify how the input variables affect the carbonation degree; therefore, as PC3 and PC4 were not representative of the carbonation degree(respective load factors: 0.074 and − 0.036), they are not depicted in the graph. For what concerns PC1, with an EV of 37.6%, η appears to be directly proportional to pressure, time, temperature and partial pressure, while the other parameters have negative load factors and, therefore, are indirectly proportional. Although a high FR should be directly proportional to η, in pressurised systems it is usually fixed to zero. Based on these considerations, PC1 seems to be well representative of pressurised systems. Along PC2, on the other hand, FR, with a high load factor, is directly proportional to η, as well as L/S, while P and t are not significative. With these specifications, PC2 can well describe the open systems, in which, as previously mentioned, temperature can positively affect the carbonation degree, but it is not possible to reach high values. The low load factors of partial pressure along these PCs can be explained by the few data of experiments carried out at different CO_2 concentrations.

Figure 12 shows the scores plot, which represents the modelled data, integrated with the loadings plot for a better interpretation of the multivariate space. Each experiment is labelled with its number from Table 3, it's filled according to the colour bar (representing the CO_2 uptake), and it's shaped according to the legend, which divides the dataset into four groups based on the type of reactor adopted. The disposition of the dataset along PC1 and PC2 allows to group back the dataset based on their reactor type, which is possible especially due to the different conditions of applicability that can be adopted. Looking again at the loadings, it is possible to notice that increasing partial pressure and temperature always affect positively the carbonation degree even if their effect is not highly significant. Concerning the response adopted, the CO_2 uptake, it is clearly disposed along with the carbonation degree and, while it is possible to individuate the same experiment with highest η and CO_2 uptake as the *19* [21], obtained with a rotating packed bed reaction, the second highest η was obtained by *24* and *25* [36] in supercritical conditions and the second highest CO_2 uptake by [37] in a pressurised reactor. In particular, the supercritical CO_2 conditions, obtained at high temperature and at the highest pressure, are well separated from the others, also due to the longest reaction time of the dataset. The good results of RPBR and IPSBR, even though at lower pressures, are obtained thanks to the ability of these reactors to maximise the contact with the CO_2 and the introduction of other, more specific parameters such as slurry flow rate, inert particles fraction and water conductivity (seawater adoption).

Pressurised systems are located in the central part of the graph and develop along the direction of η, obtaining good carbonation results at higher temperatures, pressures and CO_2 concentrations, with limited effect due to L/S. Few experiments operated in open systems are reported in the literature [17, 40] apart from this study. Open systems can only operate at ambient pressure and have a simpler setup with respect to the other reactors. Even though in these studies it was not possible to operate under pressure, thanks to the adoption of a high CO_2 flow rate, reasonable time, improved temperature and suitable liquid-to-solid ratio, the open systems path was finally similar to that of pressurised systems, along the direction of improving carbonation degree. Two different considerations drove the adoption of a low L/S ratio. In fact, even though higher L/S results in lower viscosity of the slurry and easier dissolution of CO_2, it lowers the ionic strength (together with the solubility of reactive phases [37, 41]) and produced higher volumes to be treated after the carbonation process.

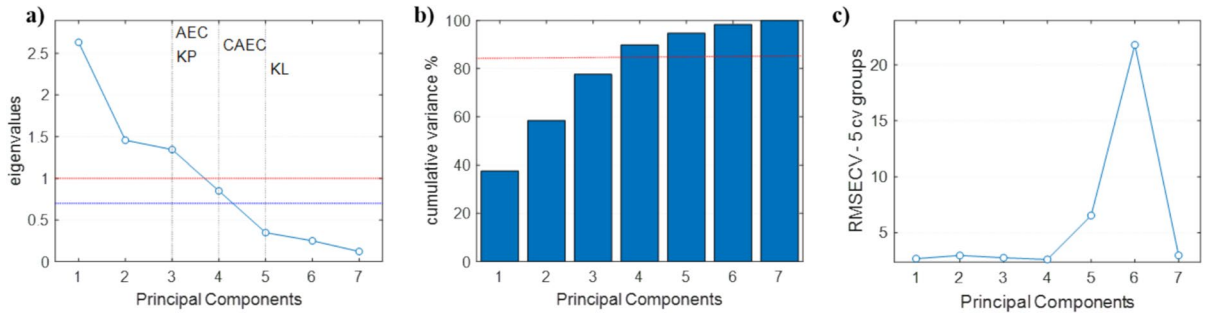

Fig. 10 Selection of optimal components for PCA: **a** Eigenvalues; **b** Cumulative variance; **c** Root mean square error of cross-validation (5 groups for venetian blinds cross-validation method)

Fig. 11 PC1 and PC2 vs variables loadings plot

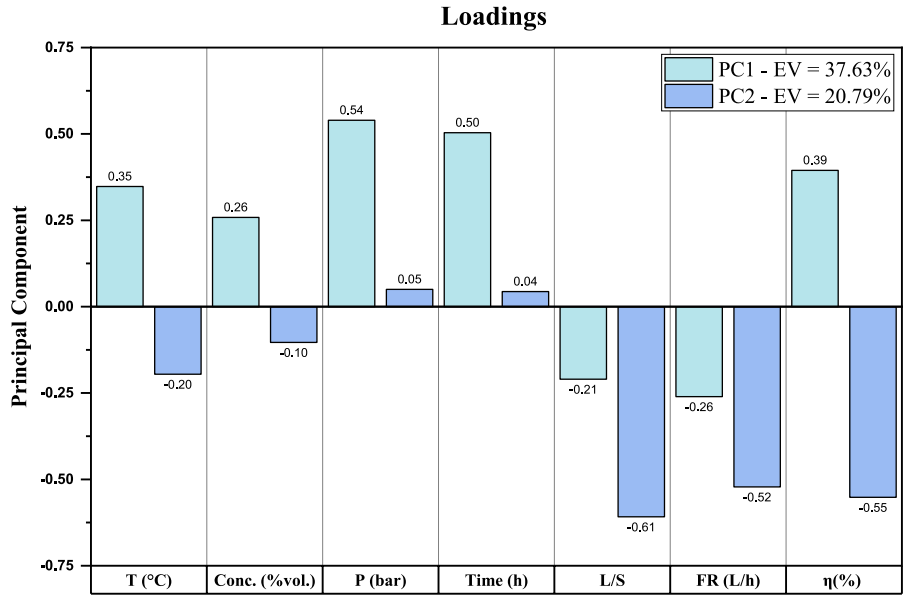

A responsible use of PCA can extract new suggestions for the improvement of EAF slag aqueous carbonation. In particular, future work could explore the combined effect of CO_2 flow rate, partial pressure and L/S or focus on the adoption of additives or high conductivity solutions, which boosted the results of Ibrahim et al. [22] at the same conditions.

4 Conclusions

This study investigated the accelerated aqueous carbonation of electric arc furnace slag in an open system. As a challenge, the goal was to enhance the CO_2 uptake capability of the slag by operating under mild conditions, with a view toward developing a low energy, industrially integrated process. To achieve this, ambient pressure, low liquid-to-solid ratio, and minimised temperature and time conditions were adopted. In order to optimise the carbonation process, while at the same time maintaining soft conditions, a design of experiments was developed.

A central composite design was adopted to evaluate the CO_2 content capacity of EAF slag and examine the individual and combined effects of the operating parameters of time and temperature on the uptake. The Response Surface Methodology showed a non-representative trend along time, therefore a non-linear model was adopted for a better prediction of CO_2 content above 50 min. The results were satisfactory with

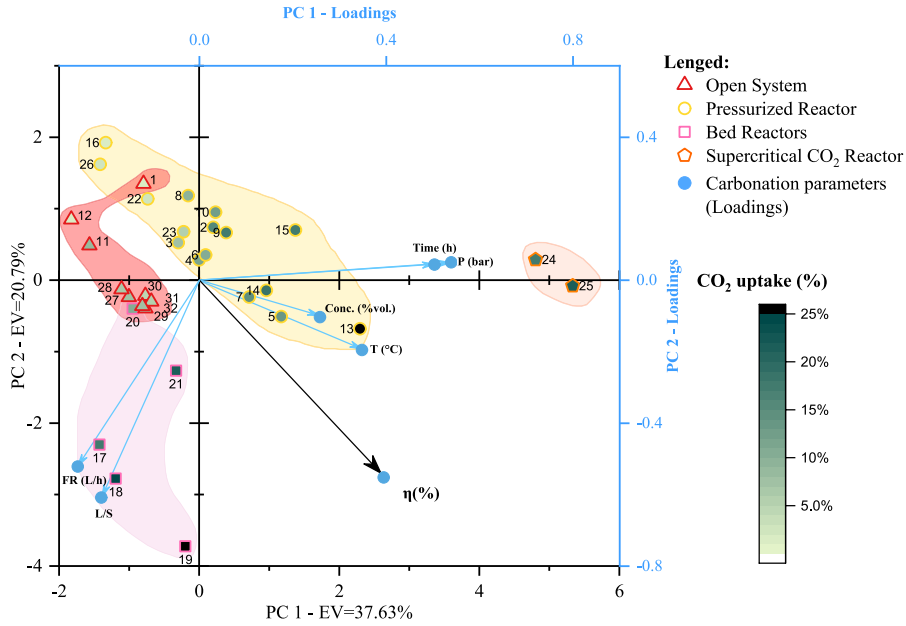

Fig. 12 Principal component analysis: scores plot

an optimum CO_2 uptake of 7.7% and the carbonation degree obtained, 30.2%, was the highest registered in previous literature for open systems.

A literature analysis on previous aqueous and wet direct carbonation of EAF slag was carried out using Principal Component analysis. This exploratory data analysis allowed to identify the most effective carbonation parameters based on the reactor type, suggesting the investigation of further parameters such as L/S and CO_2 flow rate and partial pressure for open systems, maintaining the perspective of a sustainable process. In this regard, the proposed methodology, incorporating the utilisation of the proposed experimental configuration for the construction of the RSM-based model, can be expanded to encompass the investigation of alternative operational parameters. Furthermore, this approach can be adopted for any material type to assess the carbonation efficiency of the process in relation to the parameters under consideration. Another potential approach for enhancing EAF slag CO_2 uptake, whilst maintaining an ecological perspective, involves the quantification and removal of the non-reactive metallic iron phase by magnetic separation. This strategy has been previously proposed in other studies for the recycling of iron into the steelmaking process [42]. A detailed Life Cycle Assessment analysis will be necessary to account for all the processes involved and verify the real impact of wet carbonation in terms of CO_2 emissions reduction. At the same time, further attention should be directed to the evaluation of carbonated EAF slag as supplementary cementitious material, with the ambitious goal to provide a process able to mitigate both the steelmaking and the cement industries CO_2 emissions.

Acknowledgements The research described in this paper was financially supported by the European Union's for the PON "Ricerca e Innovazione" 2014-2020 Azione IV.5—REACT EU projects (DM 1061) and by CRH Innovation Centre for Sustainable Construction Europe. The authors gratefully acknowledge the Safety of Infrastructures and Constructions (SISCON) laboratory for providing the instrumentation for thermal and granulometry analysis.

Funding Open access funding provided by Politecnico di Torino within the CRUI-CARE Agreement.

Data availability Data will be made available on request.

References

1. Van Ruijven BJ, Van Vuuren DP, Boskaljon W, Neelis ML, Saygin D, Patel MK (2016) Long-term model-based projections of energy use and CO2 emissions from the global steel and cement industries. Resour Conserv Recycl 112:15–36. https://doi.org/10.1016/J.RESCONREC.2016.04.016
2. Scrivener KL, John VM, Gartner EM (2018) Eco-efficient cements: potential economically viable solutions for a low-CO2 cement-based materials industry. Cem Concr Res 114:2–26. https://doi.org/10.1016/J.CEMCONRES.2018.03.015
3. European Committee for Standardization (2004) European Standards EN 197–1: 2000 (Amendment A1: 2004): Cement – Part 1: Composition, specifications and conformity criteria for common cements
4. Overcoming bottlenecks in steelmaking with an AOD converter. https://magazine.primetals.com/2018/03/01/overcoming-bottlenecks-in-steelmaking-with-an-aod-converter/. Accessed 7 Aug 2024
5. Singh SK, Vashistha P, Chandra R, Rai AK (2021) Study on leaching of electric arc furnace (EAF) slag for its sustainable applications as construction material. Process Saf Environ Prot 148:1315–1326. https://doi.org/10.1016/J.PSEP.2021.01.039
6. Zhang Y, Yu L, Cui K, Wang H, Fu T (2023) Carbon capture and storage technology by steel-making slags: recent progress and future challenges. Chem Eng J 455:140552. https://doi.org/10.1016/J.CEJ.2022.140552
7. Belhadj E, Diliberto C, Lecomte A (2012) Characterization and activation of basic oxygen furnace slag. Cem Concr Compos 34:34–40. https://doi.org/10.1016/J.CEMCONCOMP.2011.08.012
8. World Steel in Figures (2023)
9. World Steel in Figures (2013)
10. Skaf M, Manso JM, Aragón Á, Fuente-Alonso JA, Ortega-López V (2017) EAF slag in asphalt mixes: a brief review of its possible re-use. Resour Conserv Recycl 120:176–185. https://doi.org/10.1016/J.RESCONREC.2016.12.009
11. Gobetti A, Cornacchia G, Ramorino G (2022) Reuse of electric arc furnace slag as filler for nitrile butadiene rubber. JOM 74:1329–1339. https://doi.org/10.1007/S11837-021-05135-6/FIGURES/8
12. Primavera A, Pontoni L, Mombelli D, Barella S, Mapelli C (2015) EAF slag treatment for inert materials' production. J Sustain Metall. https://doi.org/10.1007/s40831-015-0028-2
13. Adegoloye G, Beaucour AL, Ortola S, Noumowe A (2016) Mineralogical composition of EAF slag and stabilised AOD slag aggregates and dimensional stability of slag aggregate concretes. Constr Build Mater 115:171–178. https://doi.org/10.1016/J.CONBUILDMAT.2016.04.036
14. Wang YJ, Tao MJ, Li JG, Zeng YN, Qin S, Liu SH (2021) Carbonation of EAF stainless steel slag and its effect on chromium leaching characteristics. Crystals. https://doi.org/10.3390/cryst11121498
15. Huijgen WJJ, Comans RNJ (2006) Carbonation of steel slag for CO2 sequestration: leaching of products and reaction mechanisms. Environ Sci Technol 40:2790–2796. https://doi.org/10.1021/es052534b
16. Fang Y, Su W, Zhang Y, Zhang M, Ding X, Wang Q (2022) Effect of accelerated precarbonation on hydration activity and volume stability of steel slag as a supplementary cementitious material. J Therm Anal Calorim 147:6181–6191. https://doi.org/10.1007/S10973-021-10914-Z/FIGURES/10
17. Bonenfant D, Kharoune L, Sauvé S, Hausler R, Niquette P, Mimeault M, Kharoune M (2008) CO2 sequestration potential of steel slags at ambient pressure and temperature. Ind Eng Chem Res 47:7610–7616. https://doi.org/10.1021/ie701721j
18. Baciocchi R, Costa G, Di Bartolomeo E, Polettini A, Pomi R (2011) Wet versus slurry carbonation of EAF steel slag. Greenhouse Gases: Sci Technol 1:312–319. https://doi.org/10.1002/ghg.38
19. Omale SO, Choong TSY, Abdullah LC, Siajam SI, Yip MW (2019) Utilization of Malaysia EAF slags for effective application in direct aqueous sequestration of carbon dioxide under ambient temperature. Heliyon 5:e02602. https://doi.org/10.1016/J.HELIYON.2019.E02602
20. Bonfante F, Humbert P, Tulliani JM, Palmero P, Ferrara G (2024) CO2 uptake of cement by-pass dust via direct aqueous carbonation: an experimental design for time and temperature optimisation. Mater Struct/Mater et Construct0 57:1–18. https://doi.org/10.1617/S11527-024-02457-0/TABLES/3
21. Pan SY, Chung TC, Ho CC, Hou CJ, Chen YH (2017) Chiang PC (2017) CO2 Mineralization and utilization using steel slag for establishing a waste-to-resource supply Chain. Sci Rep 7:1–11. https://doi.org/10.1038/s41598-017-17648-9
22. Ibrahim MH, El-Naas MH, Zevenhoven R, Al-Sobhi SA (2019) Enhanced CO2 capture through reaction with steel-making dust in high salinity water. Int J Greenhouse Gas Control 91:102819. https://doi.org/10.1016/J.IJGGC.2019.102819
23. Huntzinger DN, Gierke JS, Kawatra SK, Eisele TC, Sutter LL (2009) Carbon dioxide sequestration in cement Kiln dust through mineral carbonation. Environ Sci Technol 43:1986–1992. https://doi.org/10.1021/es802910z
24. Bonfante F, Ferrara G, Humbert P, Tulliani JM, Palmero P (2023) Direct aqueous mineralization of industrial waste for the production of carbonated supplementary cementitious materials. RILEM Bookseries 44:581–592. https://doi.org/10.1007/978-3-031-33187-9_54/COVER

25. Ferrara G, Belli A, Keulen A, Tulliani J-M, Palmero P (2023) Testing procedures for CO2 uptake assessment of accelerated carbonation products: experimental application on basic oxygen furnace steel slag samples. Constr Build Mater 406:133384. https://doi.org/10.1016/J.CONBUILDMAT.2023.133384
26. Bonfante F, Ferrara G, Humbert P, Garufi D, Tulliani J-MC, Palmero P (2024) CO2 Sequestration through aqueous carbonation of electric arc furnace slag. J Adv Concr Technol 22:207–218. https://doi.org/10.3151/JACT.22.207
27. Humbert PS, Castro-Gomes JP, Savastano H (2019) Clinker-free CO2 cured steel slag based binder: optimal conditions and potential applications. Constr Build Mater 210:413–421. https://doi.org/10.1016/J.CONBUILDMAT.2019.03.169
28. Liu G, Schollbach K, van der Laan S, Tang P, Florea MVA, Brouwers HJH (2020) Recycling and utilization of high volume converter steel slag into CO2 activated mortars: the role of slag particle size. Resour Conserv Recycl 160:104883. https://doi.org/10.1016/J.RESCONREC.2020.104883
29. Mahoutian M, Shao Y, Mucci A, Fournier B (2015) Carbonation and hydration behavior of EAF and BOF steel slag binders. Mater Struct 48:3075–3085. https://doi.org/10.1617/s11527-014-0380-x
30. Bezerra MA, Santelli RE, Oliveira EP, Villar LS, Escaleira LA (2008) Response surface methodology (RSM) as a tool for optimization in analytical chemistry. Talanta 76:965–977. https://doi.org/10.1016/j.talanta.2008.05.019
31. Bro R, Smilde AK (2014) Principal component analysis. Anal Methods 6:2812–2831. https://doi.org/10.1039/C3AY41907J
32. Ballabio D (2015) A MATLAB toolbox for principal component analysis and unsupervised exploration of data structure. Chemom Intell Lab Syst 149:1–9. https://doi.org/10.1016/J.CHEMOLAB.2015.10.003
33. Chen Z, Cang Z, Yang F, Zhang J, Zhang L (2021) Carbonation of steelmaking slag presents an opportunity for carbon neutral: a review. J CO2 Utiliz 54:101738. https://doi.org/10.1016/j.jcou.2021.101738
34. Bodor M, Santos RM, Kriskova L, Elsen J, Vlad M, Van GT (2013) Susceptibility of mineral phases of steel slags towards carbonation: mineralogical, morphological and chemical assessment. Eur J Mineral 25:533–549. https://doi.org/10.1127/0935-1221/2013/0025-2300
35. Lothenbach B, Durdzinski P, De Weerdt K (2018) Thermogravimetric analysis. In: A Practical Guide to Microstructural Analysis of Cementitious Materials. CRC Press, pp 196–231
36. Kim J, Azimi G (2021) The CO2 sequestration by supercritical carbonation of electric arc furnace slag. J CO2 Utiliz 52:101667. https://doi.org/10.1016/j.jcou.2021.101667
37. Baciocchi R, Costa G, Di Gianfilippo M, Polettini A, Pomi R, Stramazzo A (2015) Thin-film versus slurry-phase carbonation of steel slag: CO2 uptake and effects on mineralogy. J Hazard Mater 283:302–313. https://doi.org/10.1016/j.jhazmat.2014.09.016
38. Bonfante F, Ferrara G, Humbert P, Tulliani JM, Palmero P (2023) CO2 mineralization process of industrial by-products for the production of sustainable mortars. In: 3rd fib Symposium on Concrete and Concrete Structures, Nov 9th-10th. fib. The International Federation for Structural Concrete, pp 355–362
39. He YX, Jiao Z, Yang J (2018) Comprehensive evaluation of global clean energy development index based on the improved entropy method. Ecol Indic 88:305–321. https://doi.org/10.1016/J.ECOLIND.2017.12.013
40. Uibu M, Kuusik R, Andreas L, Kirsimäe K (2011) The CO2 -binding by Ca-Mg-silicates in direct aqueous carbonation of oil shale ash and steel slag. Energy Procedia 4:925–932
41. Huijgen WJJ, Witkamp G-J, Comans RNJ (2005) Mineral CO2 sequestration by steel slag carbonation. Environ Sci Technol 39:9676–9682. https://doi.org/10.1021/es050795f
42. Kurecki M, Meena N, Shyrokykh T, Korobeinikov Y, Jarnerud Örell T, Voss Z, Pretorius E, Jones J, Sridhar S (2024) Recycling perspectives of electric arc furnace slag in the united states: a review. Steel Res Int. https://doi.org/10.1002/SRIN.202300854
43. Baciocchi R, Costa G, Di Bartolomeo E, Polettini A, Pomi R (2010) Carbonation of stainless steel slag as a process for CO2 storage and slag valorization. Waste Biomass Valoriz 1:467–477. https://doi.org/10.1007/s12649-010-9047-1
44. Ben Ghacham A, Pasquier LC, Cecchi E, Blais JF, Mercier G (2016) CO2 sequestration by mineral carbonation of steel slags under ambient temperature: parameters influence, and optimization. Environ Sci Pollut Res 23:17635–17646. https://doi.org/10.1007/S11356-016-6926-4/FIGURES/8
45. Fang Y, Shan J, Wang Q, Zhao M, Sun X (2024) Semi-dry and aqueous carbonation of steel slag: characteristics and properties of steel slag as supplementary cementitious materials. Constr Build Mater 425:135981. https://doi.org/10.1016/J.CONBUILDMAT.2024.135981